ELSEVIER

Journal of Power Sources 67 (1997) 93–103

JOURNAL OF POWER SOURCES

The PbO_2 agglomerate-of-spheres: investigation of four grid materials

E. Bashtavelova *, A. Winsel

Universität (GhK) Kassel, Heinrich-Plett-Straße 40, 34132 Kassel, Germany

Received 1 September 1996; revised 20 October 1996; accepted 12 December 1996

Abstract

During the past decade, the agglomerate-of-spheres (AOS) model has been developed to describe the behaviour of the PbO_2 electrode during cycling. In the model, the formation of the AOS is described as an electro-metasomatic process that creates the so-called 'electroformative' force (EFF). This force causes an enlargement of the entire volume of the formed PbO_2. PbO_2 electrodes are investigated in a special electrochemical cell that is integrated into a tension testing machine. With this arrangement, the positive electrode can be cycled with simultaneous measurement of the EFF and the solid-state resistance (SSR) between the grid and the active material during formation, charge and discharge. From a technological point of view, it is of interest to investigate the influence of the grid alloy on the AOS parameters of the PbO_2 electrode. Investigations have been performed on pure lead and Pb–Sb, Pb–Ca–Sn and Pb–Ca–Sn–Ag alloys. A very small amount of additive can greatly influence the mechanical, corrosive and electrochemical properties. The corrosion behaviour depends mainly on the properties of the corrosion layer (i.e., on its mechanical, electronic, and electrochemical characteristics) rather than on the properties of the alloy itself. The components of the grid alloys appear to influence the EFF, the highest values are observed for the Pb–Sb alloy. This alloy exhibits the smallest corrosion region of the tested materials. The rupture plane after 15 cycles for all four materials is located in the active material close to the 'grid'. The tensile strength differs markedly between the different materials. A very high tensile strength is displayed by the Pb–Ca–Sn–Ag alloy. This demonstrates the influence of silver on the behaviour of the active material, although the tin content is about 35% larger, too. Theoretical consideration is given to the formation of the corrosion layer. It is concluded that no significant layer of PbO exists between grid metal and the active material. © 1997 Elsevier Science S.A.

Keywords: Agglomerate-of-spheres; Capacity; Corrosion layer; Electroformative force; Lead/acid batteries

1. Introduction

During cycling in electric vehicles, the PbO_2 electrodes of lead/acid batteries show very often a disastrous and unexpected diminution in capacity that is relaxable. Its symptoms and therapies are described as 'reversible insufficient mass utilization' (RIMU) [1,11,12]. The behaviour can be explained by the 'agglomerate-of-spheres model' (AOS model). The formation of the AOS is considered to be an electro-metasomatic process that creates the so-called electroformative force (EFF) [2]. PbO_2 electrodes are studied in a special electrochemical cell, that is integrated into a tension testing machine. With this arrangement, the positive electrode can be cycled with simultaneous measurement of the EFF and the solid-state resistance (SSR) between the grid and the active material during formation, charge and discharge [3]. From a technological point of view, it is of interest to investigate the influence of the grid material on the AOS parameters of the PbO_2 electrode. An influence is expected since materials, such as antimony and tin, have been shown [4] to effect the 'RIMU' when added to the electrolyte.

2. Experimental

2.1. Alloys

Many different lead alloys for use in negative and positive electrodes have been developed during the one-hundred years of lead/acid battery technology. Antimony, calcium, tin, tellurium and silver are common components in present technology. Even very small amounts of such components can influence markedly the mechanical, corrosive and electrochemical properties of the alloys [15]. The

* Corresponding author.

0378-7753/97/$17.00 © 1997 Elsevier Science S.A. All rights reserved
PII S0378-7753(97)02500-7

Table 1
Test electrode materials

Alloy	1	2	3	4
Specification	Pure lead	Pb–1.6 wt.%Sb	Pb–0.095 wt.%Ca-0.335 wt.%Sn	Pb–0.045 wt.%Ca-0.495 wt.%Sn-0.042 wt.%Ag

corrosion behaviour depends mainly on the properties of the corrosion layer (i.e., on its mechanical, electronic and electrochemical behaviour), rather than on the properties of the alloy itself. In co-operation with the VARTA R&D Center, pure lead and three alloys of technical importance have been prepared at VARTA's smelter plant in Krautscheid (see Table 1). From these materials, bowls and rods have been constructed; these are the special components of the test cells [3], Fig. 1. The bowls were constructed from lead-alloy sheet that was made from cast pig lead by calandering. The rods were gravity cast in a brass mould. The bowls were pasted with one batch of tribasic lead sulfate (3BS) active material.

2.2. Pasting and formation of the electrodes

Experiments were performed under the following conditions: paste density: 3.8 g cm^{-3}; weight of the unformed tablet: about 3.8 g; curing at room temperature; formation current density: 28.6 mA g^{-1}; time of formation: 24 h.

Studies were made as follows: (i) after formation, the electrode was ruptured, and (ii) the electrode was formed, cycled and then ruptured. As in former experiments, a 'good' charge current of 15 mA g^{-1} (60 mA) was fed to the PbO_2 electrode through the rod and the bowl alternately. A discharge current of 12.5 mA g^{-1} was taken from the bowl solely until the electrode potential reached 800 mV against the hydrogen electrode in the same solution. After about 15 cycles, the rod was ruptured from the tablet. Rods, bowls and tablets were subjected to scanning electron miroscopy (SME) analysis.

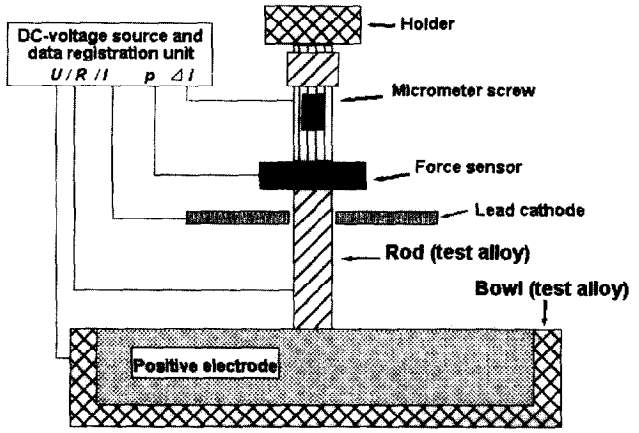

Fig. 1. Schematic view of the electrochemical cell with a bowl and a rod as the 'grid'.

3. Results

3.1. Formation

The formation process initiates the EFF. In the beginning, the zones of positive active-material (PAM) near to the rod and near to the bowl are treated by different current densities. After an electronic network of PbO_2 has been created throughout the tablet, the applied current acts more and more homogeneously on the PAM. The increase in force, dK, caused by charging an amount dQ to the electrode, can be represented by dK/dQ. This relationship is termed 'specific strengthening'; its dimension is $dK/dQ = p$ per Ah. The specific strengthening is a preliminary measure of the change in the intrinsic mechanical energy of the tablet, caused by the formation of the PbO_2. Indeed, the value of dK/dQ changes during the formation process. It often exhibits a maximum at the beginning of the formation process, so long as the PbO_2 network has not been established throughout the tablet, because in this period, 50% of the applied charge is concentrated in the neighbourhood of the rod, as mentioned before. Later on, the formation process continues homogeneously throughout the whole tablet. For comparison of the different samples, the maximum of dK/dQ after 5 h of formation was taken and defined as $(dK/dQ)_5$. A detailed theoretical investigation of this topic will be published soon. The values are listed in Table 2.

The development of the EEF during formation is different for the four materials. This can be explained by the action of the different alloy constituents. The action appears to be greatest in the first 2 h and is attributed to the corrosion of the grid, both during the curing process and in the dry state before formation.

The data given in Fig. 2 show that the behaviour of the electrodes is different. The volume of the PAM in a 45°-cylinder beneath the rod is 0.155 cm^3 or 14% of 1.07 cm^3, which is the total volume of the tablet. Its capacity is about 0.76 Ah. If the current of formation (100 mA) is fed

Table 2
In situ mechanical and resistance data of active material on different alloys after formation

Alloy	1	2	3	4
Specification	pure lead	Pb–Sb	Pb–Ca–Sn	Pb–Ca–Sn–Ag
EFF (p)	−800	−1600	−550	−1000
SSR (Ω)	0.69	0.86	0.13	0.048
$(dK/dQ)_5$ (p/Ah)	−1450	−1450	−59	−55

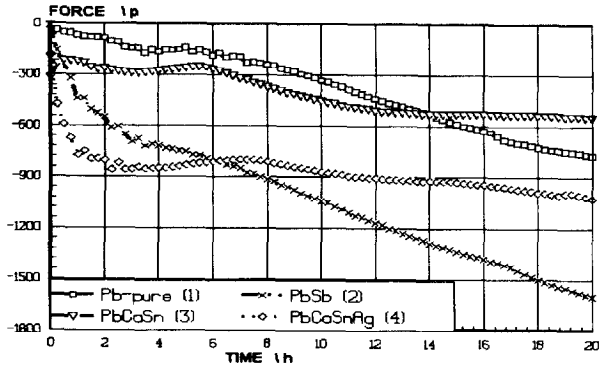

Fig. 2. Change in EFF during formation (25 mA g^{-1}) of four electrodes with different grid materials.

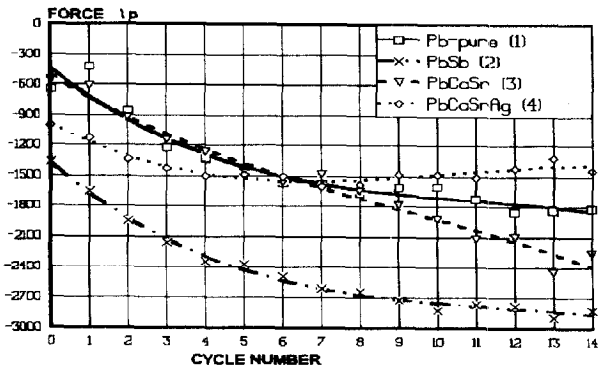

Fig. 4. EFF in charged electrodes during 15 cycles.

only through the rod, the time for bridging of the rod and the bowl should be about 1 h. In the present case, 50% of the charge is fed through the rod and 50% through the bowl. From this, a bridging time of about 2 h can be expected. During the formation time (> 6 h), the EFF in Fig. 2 develops in nearly a parallel manner for both electrodes containing calcium and tin, and likewise for the antimony-containing and pure-lead electrodes.

3.2. Cycling

The development of the EFF and the solid-state resistance (SSR) was monitored during cycling. The capacity values of all electrodes during the first 15 cycles lie in a narrow range of about 0.11 Ah g^{-1} (Fig. 3). This value corresponds to about 4.18 Ah per electrode. This is the 8-h discharge for a discharge current of 50 mA and about 55% material utilization.

3.2.1. Electroformative force measurement

The change in EFF of the charged electrodes during cycling is given in Fig. 4. The electrode with the Pb–Sb 'grid' displays the largest absolute value of the EFF during cycling. After 10 cycles, the EFF remains constant. The change in EFF with cycle number for the pure-lead and the Pb–Ca–Sn electrodes is very similar, but the absolute values of the EFF are significantly smaller than that for the Pb–Sb electrode. The variation in the EFF of the Pb–Ca–Sn–Ag electrode with cycle number is negligible. From these experiments, it is concluded that the EFF does not depend on the increasing thickness of the developing corrosion layers on the different grid alloys, but is influenced by the different corroding components, although a complete understanding of the observed behaviour has still to be found.

3.2.2. Solid-state resistance measurements

The variation of the SSR of the electrodes during discharge is shown in Fig. 5. The behaviour is similar for all electrodes. The Pb–Sb alloy exhibits larger average values of the resistance compared with others. The resistance of an electrode remains nearly constant during about 60% of the discharge, after that it increases gradually and at the end of discharge it rises rapidly.

The SSR measurements of the recharged electrodes during the first 15 cycles are summarized in Fig. 6. The electrodes with Pb–Ca–Sn and Pb–Ca–Sn–Ag alloys have a small resistance immediately after formation and the value remains constant during cycling. The electrode with the pure-lead 'grid' has a relatively high resistance after formation, but it decreases quickly and after 2–3 cycles has values similar to those shown by the Pb–Ca–Sn and Pb–Ca–Sn–Ag electrodes. In the case of the Pb–Sb 'grid', the resistance increases after the first cycle, passes through a maximum, and then decreases slowly again with a tendency to smaller values in the following cycles.

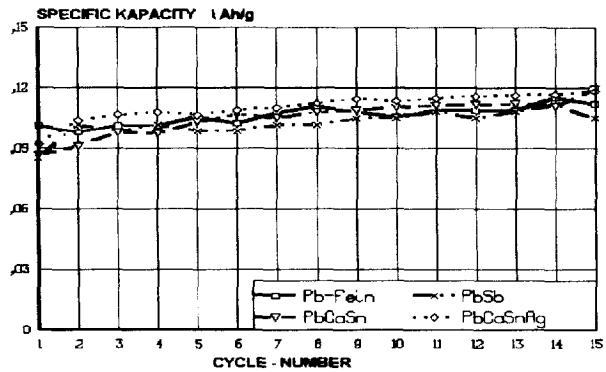

Fig. 3. Capacity of electrodes during 15 cycles.

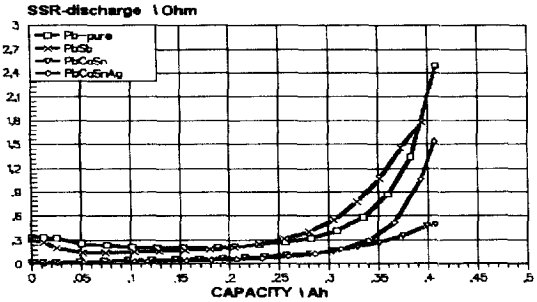

Fig. 5. Change in SSR during discharge on 15th cycle.

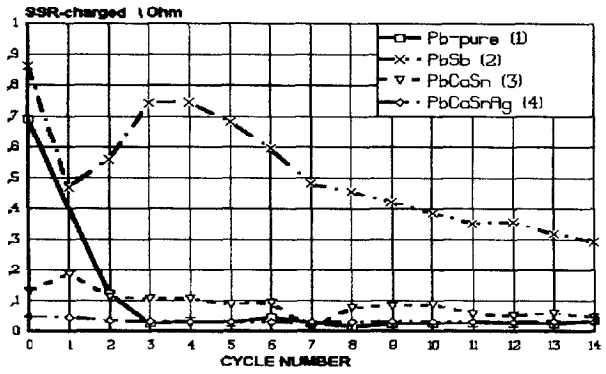

Fig. 6. Variation of SSR of charged electrodes.

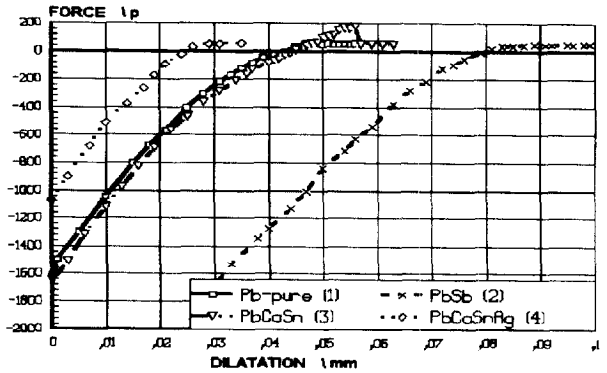

Fig. 7. Variation of EFF as a function of the dilatation during the rupture procedure after formation.

It is assumed that the differences between the samples are due to the different contributions of the 'corrosion regions' to the SSR. The reason may be the contamination of the neighbouring PAM by the corrosion products of the different alloys and its influence on the SSR, which for pure-lead is minimal. It is concluded that the behaviour during the first few cycles is determined by the forming, cracking and peeling of the growing corrosion layer.

3.3. Tensile strength measurements

After formation or after 15 cycles, the rods were ruptured from the tablets and the force between the rods and the tablets was measured as a function of the dilatation. Table 3 summarises all the measured data of the electrodes after cycling.

3.3.1. Rupture after formation

Changes in the EFF as a function of the dilatation during the rupture procedure after formation are given in Fig. 7. The electrode with the Pb–Ca–Sn alloy shows a remarkable tensile strength, see Table 2. In the pressure range, the curves of all electrodes are nearly parallel to each other. Therefore, the elastic behaviour of the PAM is nearly independent of the alloy constituents.

3.3.2. Rupture after cycling

After about 15 cycles, the rods were ruptured from the tablets and the force between rod and tablet measured as a function of the dilatation. The behaviour of the four electrodes is shown in Fig. 8. The values of the tensile strength vary with the alloy. The Pb–Ca–Sn–Ag alloy exhibits the highest value. Pure lead and Pb–Sb behave very similarly to each other. It should be noted that in the rupture experiments, the distance between the bowl and the rod is changed and the force exerted on the rod is measured. The force as a function of the dilatation (in mm) after 15 cycles for the four different grids is shown in Fig. 8.

The different curves are almost parallel, except the curve for the Pb–Sb alloy. Its unusual behaviour may be due to an uneven plane in the rotating parts of the screw that results in a periodical deviation from the linear change. The dilatation variable is linearly transformed in such a way that the new value is equal to zero when the force is equal to the weight of the rod of about 54 p. In this form, all curves converge to the point: 0 mm, 54 p. This is shown in Fig. 9. The transformation makes it obvious that the AOS exhibits Hook's law in its elastic behaviour. The constant is very similar for the different alloys although the tensile strength differs markedly. To analyze the elastic behaviour, quadratic regressions were formed for elastic parts of the rupture curves, see Fig. 10. These curves were calculated with the set of values shown in Table 4.

3.3.2.1. Interpretation of the regression terms. The linear term b is the Hook's constant. There seems to be a

Table 3
In situ mechanical and resistance data of active material on different grid alloys and thickness of the corrosion regions after 15 cycles

Alloy	1	2	3	4
Specification	pure lead	Pb–Sb	Pb–Ca–Sn	Pb–Ca–Sn–Ag
EFF, 1st cycle (p)	−1050	−1235	−660	−1338
SSR, 1st cycle (Ω)	0.20	0.54	0.08	0.035
EFF, 15th cycle (p)	−1785	−2447	−1950	−1510
SSR (Ω)	0.036	0.39	0.055	0.0247
15th cycle				
Tensile strength (p)	1013	914	1264	1714
Thickness of the corrosion region (μm)	about 35	about 18	about 55	about 30

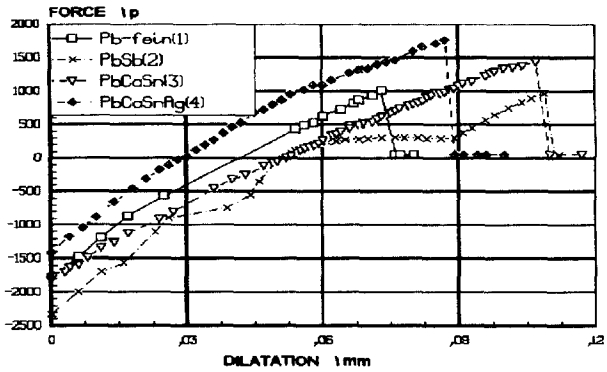

Fig. 8. Rupture curves for alloys after 15 cycles.

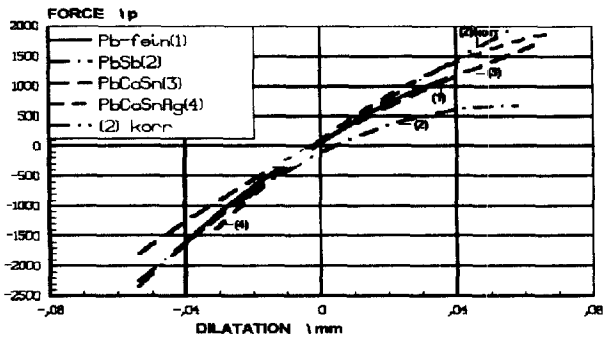

Fig. 10. Quadratic regression of rupture curves.

correlation between this elastic constant and the rupture force of the four different grid variants. Alloy 4 displays the highest value for both the elastic constant and the rupture force, while alloy 2 gives the lowest values for both parameters. The constant a gives the offset of the dilatation. It is not yet clear if there is a physical meaning of this term. The quadratic term c is related to non-linearity of elasticity due to the cross (transversal) contraction of the mass body ('bottling'). For details see Ref. [5].

3.3.3. Structure of the surfaces of ruptured corroded grid material

As an example for all alloys, Fig. 11 shows the ruptured plane on the Pb–Ca–Sn rod after formation. The AOS is formed on the very dense layer of lead dioxide and, after rupture, the remaining parts of the AOS structure are distributed like islands on the dioxide surface. It is concluded that a dense layer of lead dioxide is formed first on a smooth surface. After a first layer of particles has been formed, a second and third layer grow on the first one, mechanically and electronically connected to each other. Thus, the AOS is formed on the dense boundary layer of the grid. In the cycled electrode, the island-like distributed AOS parts cover the surface more and more. After 15 cycles, the electrodes show parts of different size covered with strongly connected AOS structures of varying thickness on the dense corrosion layers of the ruptured planes.

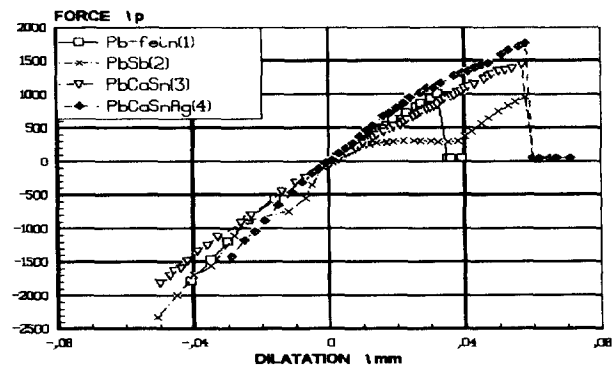

Fig. 9. Transformed rupture curves after 15 cycles.

These parts exhibit different porosity and particle size. In this case, the rupture plane is located in the active material near to the surface of the grid.

The rupture experiment after cycling of the electrodes allows the tensile strength of the necks to be calculated because, if an AOS body is ruptured into two pieces, the resulting surface is the weakest plane through the body. This plane contains the cross sections of ruptured necks only. The highest strength value is equivalent to the tensile strength of all the necks in this weakest plane.

Therefore, the tensile strength data allow a calculation of total surface area, A_h, of the necks per cm^2 and their average radius, h. The tensile strength, ϵ, in these experiments is defined as the quotient of the (positive) traction force F on the rod divided by the cross section of the total rupture plane, A, in the moment before rupture, i.e.

$$\epsilon = F/A \tag{1}$$

The number of spheres per cm^2, N, can be counted from SEM pictures. Further, each sphere (identified by a closed line in the SEM) can be expected to have had one neck to a second sphere in the pulled-off part of the electrode body. A' is identified as the total cross section of all necks within A. According to Gmelin, the tensile strength of PbO_2 is $\epsilon_{Gm} = 3 \times 10^5$ p cm^{-2} ($\pm 2 \times 10^5$ p cm^{-2}). If ϵ_{Gm} is now taken as the tensile strength of the material in the necks, then

$$A_h = A'/A = \epsilon/\epsilon_{Gm} = N\pi h^2 \tag{2}$$

$$\epsilon = N\pi h^2 \epsilon_{Gm} \Rightarrow h = \sqrt{[\epsilon/(\pi N \epsilon_{Gm})]} \tag{3}$$

The number, N, of spheres per cm^2 has been deter-

Table 4
Quadratic regression parameters of the elastic parts of the rupture curves

Dilatation ≡ X	a	b	c	Rupture force (p)
Force ≡ Y	$a+$	$bX+$	cX^2	
Alloy 1	100.52	34820	−187328	1012.7
Alloy 2	−108.35	28042	−250733	965.4
Alloy 3	83.74	30443	−81373	1445
Alloy 4	106.48	41610	−227102	1768

Fig. 11. Rupture plane after formation, Pb–Ca–Sn alloy.

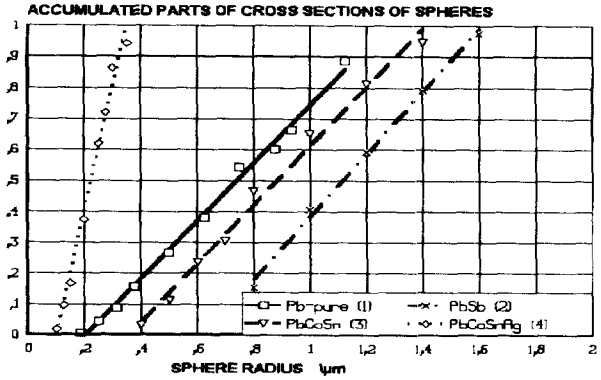

Fig. 12. Sum of the cross sections of all spheres with radii smaller than the radius on the abscissa.

mined and their radius R measured by counting of the ball-like particles in the rupture plane with the aid of a special stereo SEM photograph, Table 5. The calculated values of the quotient R/h have to be compared with the critical value $R/h < 5.9$, as calculated by Winsel et al. [1]. The stoichiometric deficiency, δ, of $PbO_{2-\delta}$ has an upper limit; this marks the existence limit of the $PbO_{2-\delta}$ in the neck zone. The deficiency in the neck zone is determined by the equilibrium between sphere and neck. Above this critical value, the neck is no longer stable.

The distribution of the number of counted spheres as a function of the sphere radius, R_i, is given in Fig. 12. $\Sigma(R)$ is taken as the accumulated cross sections of all spheres with radii smaller than R. The quotient $\Sigma(R)/\Sigma(\infty)$ is placed on the ordinate as a function of the sphere radius R. All electrodes behave similarly, except for the silver-containing one. The latter is characterized by a very large number of very small particles.

The SSR under charge conditions for the four alloys and the sum of the cross sections of the spheres are given in Table 6. This sum, $\Sigma S_{spheres}$, is almost the solid-state part of the electrode, whereas $1 - \Sigma S_{spheres}$ is the porosity. The SSR is best for the silver-containing alloy, followed by pure lead, the Pb–Ca–Sn alloy, and the Pb–Sb alloy. Fig. 13 presents some SEM photographs to show the way in which these counting results were obtained.

3.4. Corrosion layer behaviour

3.4.1. Purpose of the grid

It is the objective of the grid in both the positive and the negative electrode of a lead/acid cell to hold the active material in position and to supply it with the electrons needed for the reaction. The grid design is governed by the self-protection of the lead metal in an amount required to supply current to the active material. A second purpose is to minimize the voltage drop. The composition of the grid from lead, antimony, calcium and other components gives it the hardness to overcome the stresses during fabrication and use of the battery. All these components may influence the adhesive strength of the active material to the grid.

3.4.2. Preparation and formation of the boundary layer

After a rest time for hardening the alloy, the grid is pasted with the active material, cured, and put into the sulfuric acid. Then, the formation process takes place and establishes the boundary layer. On electrodes of both polarities, the formation process starts with the development of an electrocrystallization layer of lead or lead dioxide crystals on the surface of the grid.

Vetter [6] has calculated the range of transport of the lead ions during charge and discharge reactions based on the saturation concentration and the diffusion coefficients of the lead ions. This idea was extended at VARTA [7,8] to a 'transformation model' that is applicable to the lead

Table 5
Data for AOS

Alloy	Tensile strength (p/cm^2)	Spheres radius, R (μm)	Necks radius, h (μm)	R/h	$\Sigma N_{spheres} \times 10^6$ (cm^2)	$\Sigma N_{spheres}$ $R < 1$ μm (%)
Pure lead	2016	0.4	0.12	3.33	46.12	92.06
Pb–Sb	1828	0.9	0.19	4.74	16.03	64.08
Pb–Ca–Sn	2528	0.6	0.173	3.47	26.89	89
Pb–Ca–Sn–Ag	3428	0.18	0.056	3.12	339.12	100

Table 6
SSR under charge conditions and sum of cross sections of spheres

Alloy	SSR charge (Ω)	$\Sigma S_{spheres}$ (cm^2/cm^2)
Pure lead	0.036	0.470
Pb–Sb	0.39	0.579
Pb–Ca–Sn	0.055	0.455
Pb–Ca–Sn–Ag	0.024	0.461

sulfate and ice passivation that occur during the discharge of negative and positive electrodes. Due to the small concentration of lead ions in the electrolyte solution, the so-called 'solution-precipitation mechanism' can move solid particles of the active materials over small distances only. Therefore, it must be considered that small particles are formed first on a 'smooth' surface of the grid by electrocrystallization. After a first layer of particles has been formed, a second and third layer grow on the first and have mechanical and electronic connection to each other. In the positive electrode, the grid metal and the positive material form a short-circuit cell. Therefore, in a thermodynamic sense, the boundary layer is a region of a 'frozen non-equilibrium state', Fig. 14.

3.4.3. Thermodynamic view of the boundary layer

The frozen-in state causes the phenomenon of thermopassivation that occurs if a charged positive electrode is washed and dried at elevated temperatures. By reaction between Pb and PbO_2, a PbO layer is formed and creates a $Pb/PbO/PbO_2$ rectifier element [9], see Refs. [10–13]. In the path of the electrons during discharge, an additional voltage drop is created that vanishes after the PbO layer has disappeared by the action of the sulfuric acid. The boundary layer contributes an electronic and an electrolytic reaction path in the positive electrode and, therefore, a corresponding contribution to its resistance. The electronic path has to carry the whole current during the charge and discharge reactions. Thus, it must be very small. The

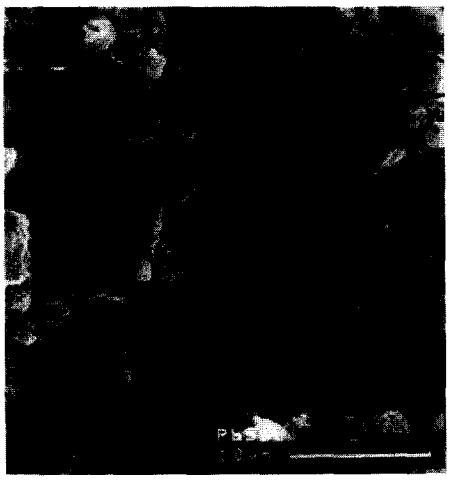

Fig. 13. SEM graphs for counting the spheres.

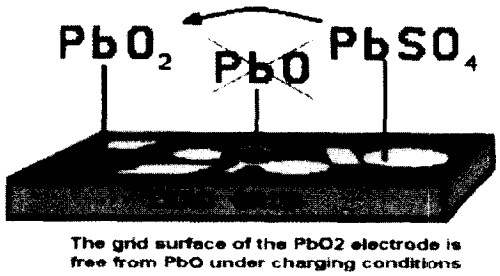

Fig. 14. Grid-layer composition at the PbO_2 potential.

electrolytic part determines the corrosion current, about 1 $\mu A\ cm^{-2}$. Consequently, it has to be very large. If the corrosion current is identified as the limiting current of the electrodialysis in the diaphragm formed by the pores of the boundary layer, the electrolytic resistance has to be in the order of 35 000 $k\Omega\ cm^2$. If the resistance is calculated on the assumption that the voltage drop of the corrosion current would consume the driving force of 2 V, the diaphragm resistance had to be in the order of 2 $M\Omega\ cm^2$, i.e. 30 times as high as the former value. The corrosion current is flowing steadily within the boundary layer. The layer can be considered to be a membrane that exhibits in its pores a large range of pH values caused by electrodialysis of the pore electrolyte [14].

The passivating boundary layer can only originate from the lead atoms of the grid itself. Thin and tight layers must have a very small porosity, due to the transformation model. This can only occur by transforming a dense layer of lead to a dense layer of lead sulfate or lead hydroxide, which the charge current transforms to PbO_2. By contrast, the PbO_2 within the active material retains the porosity of about 50% of the paste.

3.4.4. Boundary layer on the negative grid

During the discharge of a lead electrode, protecting layers of $PbSO_4$ are formed by a solution/precipitation mechanism. It is evident from the SEM pattern that these layers form a diaphragm that consists of an accumulation of mostly well-defined $PbSO_4$ crystals. This diaphragm is a transport barrier and has the following effects.

- The diaphragm contributes to the internal resistance.
- The diaphragm inhibits the diffusion of HSO_4^- species to the surface of the lead electrode where they are used for the formation of additional $PbSO_4$.
- The $PbSO_4$ formed at the surface must pass through the diaphragm away from the surface. The concentration of $PbSO_4$ is highest at the surface and lowest outside the diaphragm. Consequently, there is a tendency for $PbSO_4$ (Pb^{2+} species) to migrate through the diaphragm and to crystallize at the diaphragm/electrolyte interface. The driving force is the supersaturation of Pb^{2+} species.

By simple considerations, it can be shown that the contribution of the diaphragm to the internal resistance is

insignificant. The resistance R_δ of a diaphragm of thickness δL and porosity P is given by

$$R_\delta = \delta L/(d\sigma P^2) \quad (4)$$

The following data are assumed to be correct: diffusion coefficient, $D = 10^{-5}$ cm^2 s^{-1}; solubility, $c_0 = 2$ mg $PbSO_4$ per dm^3 $= 6.6 \times 10^{-9}$ mol cm^{-3}; porosity, $P =$ 50%; layer thickness, $\delta L = 10^{-4}$ cm; stoichiometric number, $z = 2$; Faraday constant, $F = 9600$ A s. Thus, the limiting current density of lead sulfate diffusion with supersaturation c_0 is

$$j = 2FDc_0P^2/\delta L = 32\ \mu A\ cm^{-2} \quad (5)$$

To reduce this value to 3 μA cm^{-2}, the porosity of an underlying layer of 0.1 μm thickness has to be reduced to 5%. This will occur by the corrosion process itself. The above-mentioned diaphragm, with a diffusion current density of 32 μA cm^{-2}, represents an ohmic resistance corresponding to

$$R = \delta L/\sigma P^2 = 4 \times 10^{-4}\ \Omega\ cm^2 \quad (6)$$

which, with $U = 2$ V as the driving voltage, represents a current density of

$$j = UP^2\sigma/\delta L = 5 \times 10^3\ A\,cm^{-2} \quad (7)$$

if the electrolytic conductivity within the diaphragm pores is $\sigma = 1\ (\Omega\ cm)^{-1}$. Therefore, the diaphragm resistance cannot be the limiting factor.

Equally, the diffusion of H_2SO_4 species to the electrode surface cannot be rate limiting if compared with the $PbSO_4$ (Pb^{2+}) diffusion away from the surface. There is a factor in the concentrations of these two species of about 10^6, i.e. the H_2SO_4 concentration is, under the conditions usually prevailing in a lead/acid cell, 10^6 times higher than the $PbSO_4$ concentration. Correspondingly, the H_2SO_4 (HSO_4^-) diffusion current is a million times larger than the $PbSO_4$ diffusion current. Therefore, it is assumed that the diffusion of $PbSO_4$ (Pb^{2+}) species away from the electrode surface through the $PbSO_4$ diaphragm is the rate- and capacity-determining process during corrosion. The thickness of this diaphragm increases to such an extent that finally, due to a high supersaturation at the surface, spontaneous precipitation of a $PbSO_4$ two-dimensional layer occurs. This produces a rapid voltage decay that indicates the end of discharge. The steady-state corrosion is characterized by pealing off of lead sulfate chips due to internal stress caused by the lack of volume at the surface.

3.4.5. Boundary layer as an active material

Even today, Planté positive plates (GrO) are still produced by corroding the lead surface of a filigree lead grid. After 10 cycles, the active layer is 200 μm thick and has a porosity of about 50% and a BET surface of 3 m^2 g^{-1}. The layer consists, typically, of 88.5 wt.% PbO_2, 6.9 wt.% PbO and 3.1 wt.% $PbSO_4$. Such a layer — as a homogeneous one — would exhibit a diaphragm resistance of 0.1 Ω cm^2 and would corrode very quickly. Therefore, it is concluded that the PbO_2 forms the porous outer layer on the top of a surface layer on the lead grid, from which it has originated. At first, the surface layer is dense and consists of lead hydroxide, lead sulfate and electrochemically created PbO_2. This layer causes a mechanical cracking deformation. In connection with the discharge/recharge reaction, the total porosity of the layer develops to 50%. Thus, under float conditions, lead oxide and lead sulfate can only exist in a layer of steady-state composition that is thinner than 0.1 μm with a porosity smaller than 0.5×10^{-5}.

3.4.6. Binding of the AOS to the grid

It has to be determined which layer does exist immediately on the lead surface of the grid. On the surface of an anodic polarized grid (negative electrode), a passivation layer of lead sulfate protects the metal. This consists of a porous layer on top of a two-dimensional layer of lead sulfate on the metal surface. At the PbO_2 potential, the lead sulfate is converted to PbO_2 that can grow through electronic conducting paths that emanate from the lead surface only.

The question is: Does a divalent layer of lead oxide exist between the lead surface and the PbO_2 particles? If the answer were 'Yes', this layer is too small to contribute to the internal resistance of the electrode and could only exist in those pores in which the electrodialysis controls the pH value. The acid that diffuses into this layer determines the corrosion process that is taking place all the time. Therefore, the answer should be 'No'. It should be remembered that a layer of PbO must show the X-ray pattern of lead oxide, Fig. 15.

3.4.7. Capacity of the corrosion layer in the test cell [10]

The corrosion layer holds the position between the grid and the active material. The electrons, taking part in the electrochemical reaction during charge as well as during discharge, must pass through it. Therefore, it is important that the corrosion layer consists of PbO_2 as a good electron-conducting material during all phases of charge and discharge. The corrosion layer does contribute to the capacity of the electrode in the test cell used here.

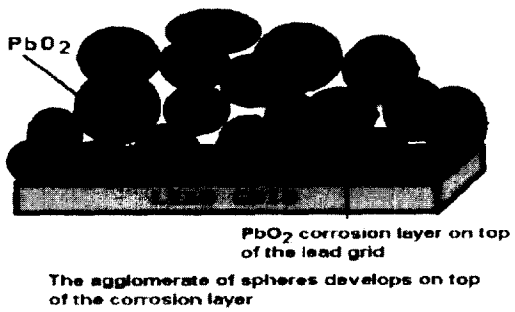

Fig. 15. PbO_2 AOS on a lead grid with a dense protecting layer of PbO_2.

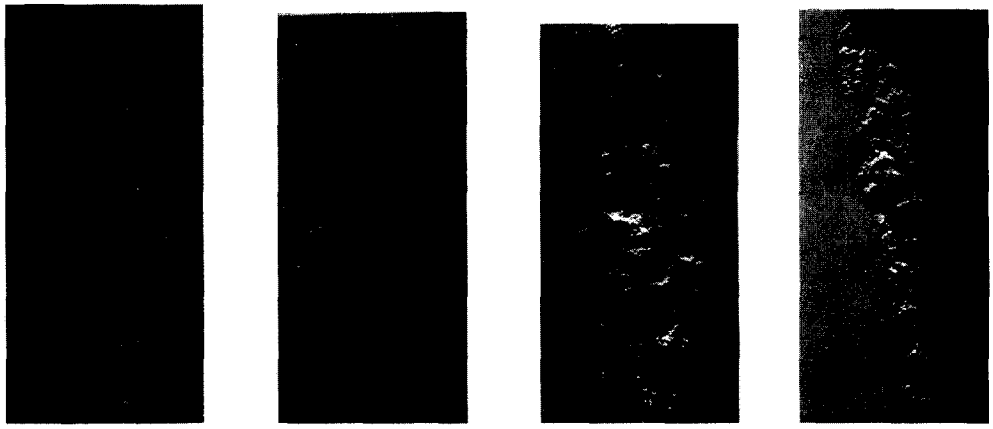

Fig. 16. Photographs of the corrosion regions of the bowls, magnification ×200.

3.4.8. Calculations

The grid surface A: $A_{ROD} = \pi R_1^2 = 3.1418 \times 0.4^2 = 0.5027\ cm^2$

$A_{bowl} = 2\pi R_2 D + \pi R_2{}^2 = 13.33\ cm^2$

$A_{bowl}/A_{rod} = 26.52$

Volume of the tablet: $V_{tab} = \pi R_2{}^2 D = 2.628\ cm^3$

Weight of the tablet: $G_{tab} = 3.2$ g

Capacity of the tablet: $C_{tab} = 9\ h \times 0.05\ A = 0.45$ Ah

Specific values:

- capacity per unit volume: $C_{tab}/V_{tab} = 0.45$ Ah/2.628 $cm^3 = 0.1712$ Ah cm^{-3}
- capacity per unit weight: $C_{tab}/G_{tab} = 0.45$ Ah/3.2 g = 0.141 Ah g^{-1}

Capacity of the 'corrosion layer'

- thickness per unit capacity: $D/C_{tab} = 0.22$ cm/0.45 Ah = 0.489 cm Ah^{-1}
- capacity per unit thickness: $C_{tab}/D = 1/0.489$ Ah $cm^{-1} = 2.045$ Ah $cm^{-1} = 736.2$ mA s μm^{-1}

The capacity of a '1 μm corrosion layer' on the bowl: $C_{1\mu} = 736.2$ mA s; this capacity holds 50 mA for $t_{1\mu} = 14.72$ s.

The capacity of a '1 μm corrosion layer' on the rod: $C_{1\mu} = 27.76$ mA s; this capacity holds 50 mA for $t_{1\mu} = 0.56$ s.

A float current, established for a PbO_2 electrode to conserve its charge, converts $PbSO_4$ to PbO_2 as quickly as it is formed by corrosion. Therefore, we can consider this layer to be a dense one. In a GrO electrode, the self-discharge under open-voltage conditions proceeds with about 3 μA cm^{-2}. This current density corresponds to a corrosion current limited by a diaphragm layer of 0.1 μm thickness and 5% porosity.

3.4.9. Experimental results

3.4.9.1. Thickness of the corrosion region of different alloys. After cycling 15 times and breaking of the PbO_2 tablets, the different bowls were cast in epoxy-resin and

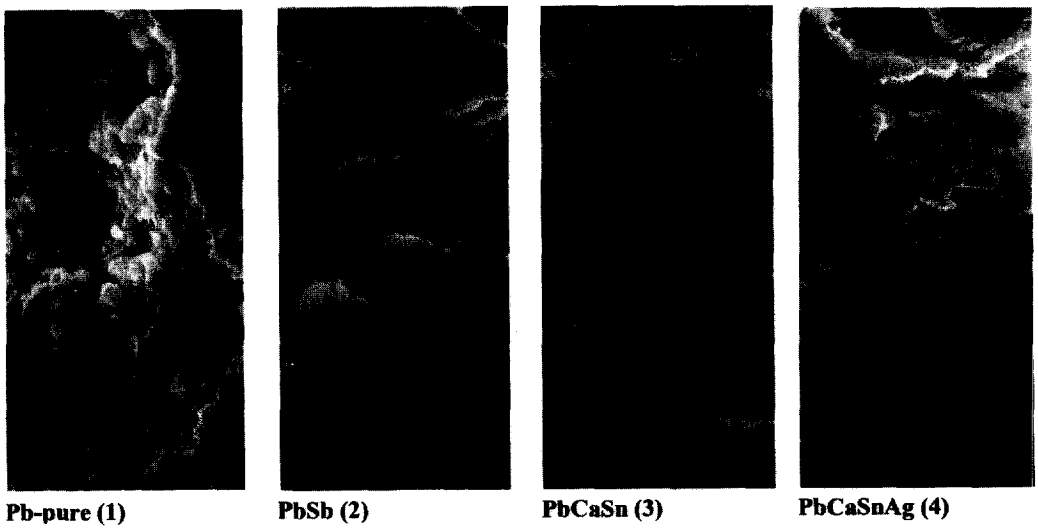

Fig. 17. SEM graphs of the corrosion layers.

microtom-cuts made perpendicular to the corrosion layers. The thickness of the corrosion region was determined by SEM analysis. These values are shown in the last row of Table 3 which, as a summary, contains the other measured parameters, too. Fig. 16 presents photographic pictures of the corrosion regions of the bowls of the four alloys at a relatively small magnification of 200. The sample of the bowl made from the Pb–Sb alloy shows the smallest thickness of the corrosion region compared with the others. The corrosion layer is dense and is distributed regularly on the metal surface. The corrosion region of the Pb–Ca–Sn–Ag alloy is similar to that of Pb–Sb, but it is more porous and thicker. The largest corrosion region is shown by the Pb–Ca–Sn 'grid'. It is porous and not distributed regularly on the metal surface. In the case of the pure-lead grid, many large cracks occur close to the metal surface and within the corrosion region, that is distributed not very regularly on the metal surface.

Interesting information about the structure of the corrosion regions of the different alloys is provided by the electron micrographs in Fig. 17(a)–(d). The pure-lead sample, as well as the Pb–Sb sample, has dense corrosion zones with cracks close to the metal surface. The pure-lead sample exhibits the largest cracks (Fig. 17(a)). The front of the corrosion zone of the Pb–Sb sample advances, wedge-like, deep into the metal (Fig. 17(b)). The development of the cracks causes strong internal stress. The corrosion zones of the Pb–Ca–Sn and Pb–Ca–Sn–Ag samples are comparatively more porous with better developed crystal structures (Fig. 17(c), (d)). An important difference is found in the transition layer metal/corrosion zone. The addition of silver to the alloy disperses probably the structure of the lead alloy and increases the adhesion to the metal surface and the compactness of the corrosion layer close to the grid (a well developed, dense, AOS structure, see Fig. 17(d)).

By applying the WDX (wavelength dispersive X-ray spectroscopy system) method of SEM analysis, the appearance of lead sulfate as a component of the different charged corrosion regions has been examined. No lead sulfate was detected in the corrosion regions.

3.4.9.2. Structure of the corrosion region of different alloys. The alloying components must not adversely affect the mechanical and electronic contact between the active material and the grid. The oxidized components of the alloy must not increase the electric resistance of the PAM and must not passivate the active material. The adhesion of the corrosion region in both directions to the grid, as well as to the active material, must also not be adversely affected.

4. Conclusions

Several different lead alloys for use in negative and positive electrodes have been developed during the one-hundred years of battery technology. Antimony, calcium, tin, tellurium and silver are the common constituents in present technology. Even very small amounts of the constitutents can greatly influence the mechanical, corrosive and electrochemical properties [15,16]. The corrosion behaviour depends mainly on the properties of the corrosion layer, i.e., on its mechanical, electronic and electrochemical characteristics.

The EFF, as a property of the PAM, exists for all tested grid materials. The constituents of the grid alloys appear to influence the EFF. There is a good correlation between the thickness of the corroded grid material and the development of the EEF, except for the Pb–Sb alloy. The tensile strength after 15 cycles differs markedly (by a factor of two) between the tested alloys, although the rupture plane is not identical with the corrosion zone, but is located in the active material close to the surface of the rod. The very high tensile strength of the electrode with the Pb–Ca–Sn–Ag alloy, compared with the alloy without silver, appears to confirm the influence of silver on the behaviour of the PAM, although the tin content is about 35% larger, too. The same can be deduced from the SSR of the charged electrodes; the lowest values were observed for the silver-containing grid. Theoretical considerations about the creation of the corrosion layer are reported. It is concluded that no real layer of PbO exists between the grid metal and the PAM.

Acknowledgements

The European Commission has financed the work as a part of the Brite–Euram Project 7297 of the Advanced Lead–Acid Battery Consortium. Special thanks are due to the Project Manager, Mr Allan Cooper, and to the contractor, VARTA Batterie AG, for supporting this work. The authors are also grateful to the following staff at the VARTA R&D Center: Dr E. Meissner for many discussions and suggestions; Mr J. Vollbert for the preparation of the rods and the bowls and for electrode pasting; Mrs H. Schöder for metallurgical cuts and preparation; Mr D. Metzeltin for SEM studies. At the University of Kassel, Mr. K.-H. Otto and the workshops have assisted the work very effectively.

References

[1] A. Winsel, E. Voss and U. Hullmeine, *J. Power Sources, 30* (1990) 209–226.
[2] A. Winsel and E. Bashtavelova, *J. Power Sources, 46* (1993) 211–217.
[3] E. Bashtavelova and A. Winsel, *J. Power Sources, 46* (1993) 219–230.
[4] E. Voss, U. Hullmeine and A. Winsel, *J. Power Sources, 30* (1990) 33.
[5] H. Höpfinger and A. Winsel, *J. Power Sources. 55* (1995) 143–152.

[6] K.J. Vetter, *Chem.-Ing. Techn., 45* (1973) 312.
[7] A. Winsel, E. Voss and U. Hullmeine, *J. Power Sources, 2* (1977/78) 878.
[8] W. Kappus and A. Winsel, *J. Power Sources, 8* (1982) 159–173.
[9] J. Garche, *J. Power Sources, 36* (1991) 405–413.
[10] A. Winsel, *ALABC Meet., Montreux, Switzerland, 1994.*
[11] E. Meissner, J. Schulz, F.-J. Glasner, D. Pavlov, G. Papazov, B. Bojinov, B. Monahov, T. Rogachev and St. Ruevski, Improvement of Cycle Life, especially under EV Discharge and Recharge Conditions, *ALABC Project AMC 004*, VARTA R&D Center and CLEPS, Final Rep., Feb. 1995.
[12] E. Meissner, *The Reversible Capacity Decay of Lead Dioxide Electrodes — A Review*, Appendix to Ref. [11].
[13] T.G. Chang, *J. Electrochem. Soc., 131* (1984) 1755-1762.
[14] P. Ruetschi and R.T. Angstadt, *J. Electrochem. Soc., 105* (1985) 555.
[15] N. Bagshaw, *Proc. 16th Int. Power Sources Symp., Bournemouth, UK, 1988.*
[16] R.D. Prengaman, *J. Power Sources, 53* (1995) 207–214.